Vol. 19, Sup. 1 (2020) 445-456
Revista Mexicana de Ingeniería Química

Determination of kinetic parameters of nucleation and growth of acetylsalicylic acid crystals in ethanol

Determinación de los parámetros cinéticos de nucleación y crecimiento de cristales de ácido acetilsalicílico en etanol

X.M. Medina-Galván*, P.A. Quintana-Hernández, J.N. Reyes-Valadez, L.F. Fuentes-Cortés

Departamento de Ingeniería Química. Tecnológico Nacional de México en Celaya. ITC. Antonio García Cubas Pte. # 600 esq. Av. Tecnológico, Celaya, Guanajuato, 38010, México

Received: April 16, 2020; Accepted: July 11, 2020

Abstract

In this work, nucleation and growth rates, as well as kinetics parameters, for the acetylsalicylic acid (ASA) -ethanol system were evaluated from experimental data and a nonlinear optimization model. Saturated solutions, between 298.15 K and 313.15 K, were prepared and cooled following linear profiles at 9, 12 and 15 K/h. Measurements online of temperature, density and crystal size distribution were registered every 30 seconds. At the end of each run, crystal dimensions were measured from images obtained with an optical microscope. The predicted results related to the concentration profile of ASA were in good agreement with the experimental data. They showed that an increment in cooling rate enhanced growth but inhibited nucleation. Similar results were obtained for an increment in the solution initial saturation concentration. The analysis of the kinetic exponents suggested crystal growth was dominated by surface diffusional effects and formation of new nuclei was dominated by primary nucleation. The images obtained with an optical microscope showed no morphological differences due to the different operation conditions. Specific shape factor evaluation confirmed the absence of morphological changes in the ASA crystals at the analyzed conditions in this study.

Keywords: acetylsalicylic acid, batch crystallization, crystallization kinetics, growth, nucleation, parameter optimization.

Resumen

En este trabajo, se evaluaron las velocidades de nucleación y crecimiento, así como los parámetros cinéticos, para el sistema de ácido acetilsalicílico (ASA) -etanol a partir de datos experimentales y un modelo de optimización no lineal. Se prepararon soluciones saturadas, entre 298.15 K y 313.15 K, y se enfriaron siguiendo perfiles lineales a 9, 12 y 15 K / h. Se obtuvieron mediciones en línea de temperatura, densidad y distribución del tamaño de los cristales y se registraron cada 30 segundos. Al final de cada experimento, se midieron las dimensiones del cristal a partir de imágenes obtenidas con un microscopio óptico. Los resultados calculados, relacionados con los perfiles de concentración, tuvieron una buena concordancia con los resultados experimentales. Estos resultados mostraron que un incremento en la velocidad de enfriamiento aumentaba el crecimiento, pero inhibía la nucleación. Se obtuvieron resultados similares para un incremento en la concentración de saturación inicial de la solución. El análisis de los exponentes cinéticos sugirió que el crecimiento de los cristales estaba dominado por los efectos de difusión superficial y la formación de nuevos núcleos estaba dominada por la nucleación primaria. Las imágenes obtenidas con un microscopio óptico no mostraron diferencias morfológicas debido a las diferentes condiciones de operación. La evaluación del factor específico de forma confirmó la ausencia de cambios morfológicos en los cristales de ASA a las condiciones analizadas en este estudio.

Palabras clave: ácido acetilsalicílico, cristalización por lotes, cinéticas de cristalización, crecimiento, nucleación, optimización de parámetros

1 Introduction

The acetylsalicylic acid (ASA) is known for its medical importance as an anti-inflammatory, antipyretic, and antiplatelet agent. The reaction of salicylic acid with acetic anhydride in liquid phase, in the presence of sulfuric acid as a catalyst, produces ASA. In addition to ASA, ethanol appears as a byproduct in the reaction that lasts approximately three hours and reaches a yield of close to 90%.

* *Corresponding author. E-mail*: xochitl.medina@iqcelaya.itc.mx
Tel. +52-46-11-29-67-10, Fax 46-16-11-75-75
https://doi.org/10.24275/rmiq/Cat1574
ISSN:1665-2738, *issn-e*: 2395-8472

ASA crystals are filtrated, dissolved in a more selective solvent and recrystallized to improve their purity (Medina-Galvan, 2018). ASA crystals are poorly soluble in water, and partially soluble in ethanol-water mixtures (Eder *et al*., 2012; Maia and Guilietti, 2008). ASA solubility considerably increases in anhydrous ethanol (Medina-Galván, 2018). ASA is also partially soluble in mixtures of salicylic acid-acetic anhydride (Xiong, *et al*. 2018) and ethanol-water-carbon tetrachloride (Göczo, 2000).

The commercial ASA crystals are tetragonal (prism-shaped), with different particle size distributions. In general, they have poor flow and compressibility properties due to the crystal habit and electrostatic charge (Göczo, 2000) and its use in a direct table-making process becomes difficult. However, the use of wet granulation, the application of special excipients or the improvement of flowability, coercibility and tabletability via the knowledge of the crystal habit make the table-making process possible. Crystal habit can be manipulated with the knowledge of some thermodynamic properties (solubility, metastable zone width, crystal growth and nucleation rates, etc.) and mathematical relationships that allow the adequate manipulation of operation variables (Kashchiev *et al*., 2010; Miyasaka, 2006; Polat and Sayan 2017; Quintana-Hernandez *et al*., 2016; Sanchez-Sanchez *et al*., 2017, 2020; Singh and Ramkrishna 2013).

Rawlings *et al*. (2002) describe the mathematical modeling for batch cooling crystallization based on population, mass and energy balances and constitutive relations for growth and nucleation kinetics. Some theoretical models have been developed for analyzing the nucleation and growth phenomena. Mulling (2001) shows a relation for homogeneous nucleation. Söhnel and Garcide (1992) present other for heterogeneous nucleation. O'Hara and Reid (1973) report some relationships for crystal growth based on Diffusion-Reaction, Spiral Dislocation or BCF and Birth and Dissemination (B&S) models. Unfortunately, these models cannot predict a priori the values of the kinetic parameters. In most cases, these parameters are empirically correlated for every particular system using experimental information obtained in either continuous or batch crystallizers.

Mixed-suspension mixed-production removal (MSMPR) crystallizers are the most commonly used for continuously operated crystallizers (Garcide and Shah, 1980). Experiments are done at different residence times and kinetic parameters are estimated from direct relationships between volumetric hold-up, mean crystal size, and mean residence time. On the other hand, batch runs are more difficult to control but allow investigations to work over wider ranges of supersaturation. Three routes for evaluating kinetic parameters for power law-type equations are reported in the literature using data obtained from batch crystallization experiments (Qiu and Rasmuson, 1994; Zhang, *et al*., 2017). The first route uses direct measurements on individual crystals (Monaco and Rosenberger, 1993); this approach is slow, expensive and not very reproducible. The second one, it uses online measurements to determine the mass and size distribution of the crystals (Wey, 1985). In the third route, a crystallization mathematical model is used to simulate the process and the calculated results are compared against experimental results. The kinetic parameters are determined by means of an optimization process. This route provides a framework for dispersed phase systems, describing the characteristic of the particles over the time and allowing the joint evaluation of nucleation and growth (Liang and Hartel, 1991, Quintana-Hernández *et al*., 2004, Frawley *et al*., 2012, Jin *et al*., 2019).

In this work, a combination of the second and third routes is proposed for evaluating the crystallization kinetic parameters for the ASA-ethanol system at different operation conditions. Saturated solutions of ASA in ethanol, between 298.15 K and 313.15 K, are prepared and cooled following linear profiles in the range of 9 to 15 K/h. On-line temperature, density and crystal-size-distribution measurements generate a set of experimental results used for calculating nucleation and crystal growth. The effects of cooling rate and saturation concentration are investigated. A nonlinear optimization algorithm for estimating the kinetic parameters is used, and it is validated by comparing the measured solution concentration profile with calculated results. Finally, microscopic images of crystals obtained at the end of each experiment are used for a morphological qualitative analysis and quantitative determination of crystal dimensions and surface shape factors.

2 Kinetic modeling

2.1 *Estimation of solubility of ASA in ethanol*

Acetylsalicylic acid solubility, c_s (g ASA/cm^3 ethanol), is evaluated using Eq. (1), where x is

the mole fraction of ASA in the mixture and it is evaluated with Eq. (2) (Maia and Giulietti, 2008). Ethanol density, ρ_E (g/cm^3), is evaluated with Eq. (3) (Medina-Galván, 2018). $T' = T/T_r$ is a dimensionless temperature in Eq. (2), T is the solution temperature (K) and $T_r = 1$ K is a reference temperature that makes dimensionless the independent variable in Eq. (2). MW_{ASA} and MW_E, are the molar masses of ASA and ethanol respectively.

$$c_s = \left(\frac{x}{1-x}\right)\rho_E \frac{MW_{ASA}}{MW_E} \tag{1}$$

$$\log(x) = 27.769 + \frac{-2500.906}{T'} - 8.323\log(T') \tag{2}$$

$$\rho_E = -1.042\times10^{-3}T + 1.101 \tag{3}$$

Eqs. (1)-(3) are valid in the range of temperature from 276.3 to 336.6 K.

2.2 Dynamic crystallization model

A batch cooling crystallization process is an unsteady-state process in which the concentration of the solute c (g solute/cm^3 solvent), population density n (# of crystals/cm^3 solution), and crystal size l (cm) change with time t (s). If agglomeration, attrition and breakage are neglected, the population balance for a well-mixed constant volume batch cooling crystallization process is represented by Eq. (4) (Quintana-Hernández, *et al*., 2004).

$$\frac{\partial n(l,t)}{\partial t} + G(t)\frac{\partial n(l,t)}{\partial l} = 0 \tag{4}$$

where G is the size-independent crystal growth rate. The initial conditions, used to integrate the population balance, follow from the ideas that at time cero there are no crystals in the solution, Eq. (5) and the minimum crystal sized detected by the measuring device is n_0, Eq. (6).

$$n(l,0) = 0 \tag{5}$$

$$n(t,0) = n_0 \tag{6}$$

For solving the population balance, Eq. (4) is converted to a system of ordinary differential equations using the method of moments (Halburt and Katz, 1964; Randolph and Larson, 1988) defined by Eq. (7).

$$M_i = \int_0^\infty n(l,t)l^i dl \tag{7}$$

Jerauld *et al*. (1983) showed that the population balance could be adequately represented by the first four distribution moments (M_0-M_3). These moments were associated with physical parameters of the process. Moments zero, one, two and three corresponded to the number of crystals (N), the total length (L), the total area (A) and the total volume (V) per unit volume of the solution respectively. Applying the definition given by Eq. (7) to the population balance, the first four moments of distribution are given by eqs. (8)-(11).

$$\left.\frac{dM_0}{dt}\right|_{L\to0} = B \tag{8}$$

$$\frac{dM_1}{dt} = 1GM_0 \tag{9}$$

$$\frac{dM_2}{dt} = 2GM_1k_s \tag{10}$$

$$\frac{dM_3}{dt} = 3\rho_{ASA}GM_2\frac{k_v}{k_s} \tag{11}$$

where B is the nucleation rate (# crystals/cm^3 s), G is the growth rate (cm/s), ρ_{ASA} is the ASA density (1.40 g/cm^3), k_s is the surface shape factor, Eq. (12) and k_v is the volume shape factor, Eq. (13). For prism-shape crystals with side dimensions a, b and c ($a > b, c = b$) the shape factors can be evaluated as follows:

$$k_s = \frac{S_c}{L^2} = \frac{4ab + 2b^2}{L^2} \tag{12}$$

$$k_v = \frac{V_c}{L^3} = \frac{ab^2}{L^3} \tag{13}$$

where S_c is the crystal area, V_c is the crystal volume and L is the characteristic crystal length. An additional relationship can be obtained for the specific surface shape factor (F), Eq. (14).

$$F = \frac{k_s}{k_v} \tag{14}$$

The constitutive relations commonly used for engineering purposes (Rawlins *et al*., 2002; Frawley *et al*., 2012; Bolaños *et al*., 2018) are semi-empirical relations as function of relative supersaturation and temperature incorporated with an Arrhenius-type expression. Eq. (15) is used for evaluating the nucleation rate.

$$B = k_{b0}\exp\left(-\frac{E_b}{RT}\right)S_r^b \tag{15}$$

where S_r represents the relative supersaturation $(c - c_s)/c_s$; k_{b0} (# crystals/cm^3 s), E_b (J/mol) and b are the frequency factor, activation energy and relative

supersaturation exponent of nucleation rate. R is the ideal gas constant (8.3144 J/mol K) and T is the solution temperature (K). For a size-independent growth rate, Eq. (16) is applied.

$$G = k_{g0} \exp\left(-\frac{E_g}{RT}\right) S_r^g \tag{16}$$

where k_{g0} (cm/s), E_g (J/mol) and g are the frequency factor, activation energy and relative supersaturation exponent of growth rate. The model is completed with the mass balance equation that relates the mass transferred from the solution to the solid phase, Eq. (17) with initial condition $c(0) = c_0$.

$$\frac{dc}{dt} = \frac{d(\rho_{ASA} M_3)}{V_E dt} = \frac{\rho_{ASA}}{V_E}\frac{dM_3}{dt} = -3\frac{\rho_{ASA}}{V_E} G M_2 V_s \frac{k_v}{k_s} \tag{17}$$

where V_E and V_S are the ethanol and solution volumes respectively. In addition, the model includes an equation for the variation of temperature as function of time. Eq. (18) represents the relation between the solution temperature and the cooling rate, R_c with initial condition $T(0) = T_0$.

$$\frac{dT}{dt} = -R_c \tag{18}$$

3 Methodology

3.1 Materials

Acetylsalicylic acid (CAS No. 50-78-2) with mass purity of 99% w/w and anhydrous ethanol (CAS No. 64-17-5) with purity of 99% w/w, both Golden Bell brand, were used in this work.

3.2 Experimental equipment

Experimental data was obtained in a stainless-steel crystallizer of three-liter capacity Pignat brand (Pilot Unit No. 9312122, Pignat, France). The crystallizer had a cooling jacket connected to a LAUDA RP1800 thermal bath (Lauda-Königshofen, Germany). Stirring speed was controlled with a RW20DZM shaker from Janke & Kunkel (USA), and transport of the solution through the equipment was done with an Easy-Load Master Flex peristaltic pump model 77201-62.

Particle size distribution was measured with a Mastersizer S (Malvern Instruments Ltd. England) with a detection range between 0.5-880 μm. Density and temperature of the solution were measured with a mPDS2000 densitometer (Anton Paar, Austria). Fig. 1 shows the schematic diagram of the equipment used.

The crystal habit at the end of each experiment was observed using an optical microscope Iroscope MG-11TFC #982262 (Mexico). Crystal dimensions were measured from the microscope images taken. The image observation field had a diameter of 500 μm.

3.3 Experimental procedure

3.3.1 Concentration of ASA in the solution

Concentration of ASA in the solution (c, g/cm^3) was evaluated based on the online density (ρ, g/cm^3) and temperature (T, °C) measurements using the linear model developed by Medina-Galván (2018), Eq. (19).

$$c = 3.686\rho + 0.0037T - 3.014 \tag{19}$$

3.3.2 Crystallization experiments

Experimental data for the evaluation of the kinetic parameters were obtained in two sets of experiments. In the first one, saturated solutions at a constant concentration of 0.2970 g/cm^3 were cooled at 9, 12 and 15 K/h. In the second one, saturated solutions at different concentrations 0.2031, 0.2463, 0.2970 and 0.3562 g/cm^2 were cooled at a constant rate of 12 K/h. The saturated solutions were prepared with 1500 cm^3 of ethanol and the corresponding mass of ASA as shown on Table 1. The saturated solutions were heated 10 K above their saturation temperature for 30 minutes ensuring their complete dissolution. For reproducible mixing conditions, the agitation rate was kept constant at 300 rpm during all experiments.

Table 1. Molar fraction, mass and solubility of acetylsalicylic acid solutions in ethanol at different temperatures, prepared in a volume of 1500 cm^3 of ethanol measured at 289.15 K.

T	x_{ASA}	m_{ASA} (g)	c (g/cm^3)
298.15	0.0611	304.70	0.2031
303.15	0.0732	369.59	0.2463
308.15	0.0869	445.59	0.2970
313.15	0.1025	534.31	0.3562

Experiments were performed by triplicate at every experimental condition and the variables temperature, density and crystal size distribution were recorded every 30 seconds.

3.4 Parameters estimation

The mass of ASA, m_{ASA}, transferred from the solution to the solid phase was calculated with Eq. (20).

$$m_{ASA} = (c - c_s)\frac{m_E}{\rho_E} \tag{20}$$

where m_E and ρ_E are the mass and density of ethanol. Moment three, defined as the volume of ASA per unit of solution volume, was evaluated using Eq. (21).

$$M_3 = \frac{V_{ASA}}{V_s} = \frac{m_{ASA}}{\rho_{ASA} V_s} \tag{21}$$

Moments 2, 1 and 0 were calculated using M_3 and the online measurement of diameters D_{32}, D_{21} and D_{10}, eqs. (22)-(24).

$$M_2 = \frac{M_3}{D_{32}} \tag{22}$$

$$M_1 = \frac{M_2}{D_{21}} \tag{23}$$

$$M_0 = \frac{M_1}{D_{10}} \tag{24}$$

Experimental nucleation and growth rates were calculated for each sampling time, k, with Eq. (25) and Eq. (26) respectively.

$$B_{k+1} = \frac{M_{0,k+1} - M_{0,k}}{t_{k+1} - t_k} \tag{25}$$

$$G_{k+1} = \frac{D_{43,k+1} - D_{43,k}}{t_{k+1} - t_k} \tag{26}$$

The kinetic parameters (k_{b0}, b, E_b, k_{g0}, g, E_g) were obtained with a nonlinear optimization algorithm that used the described kinetic model and the Marquardt-Levenberg method (Matlab instruction lsqnonlin). The system of differential equations eqs. (8)-(11), (17) and (18) was solved numerically by means of the fourth order Runge-Kutta method (Matlab instruction ode45).

4 Results and discussion

4.1 Experimental nucleation and growth rates evaluation

Fig. 2a shows the concentration profiles (saturated solution at 0.2970 g/cm^3) at three different cooling rates (9, 12 and 15 K/h). Experiments with low cooling rate exhibit a larger lag before nucleation appears. This lag generates an increment in the relative supersaturation, as shown in Fig. 2b. Figures 2c and 2d show the growth and nucleation profiles. The maximum values for growth and nucleation are reached when the relative supersaturation reaches the maximum value too.

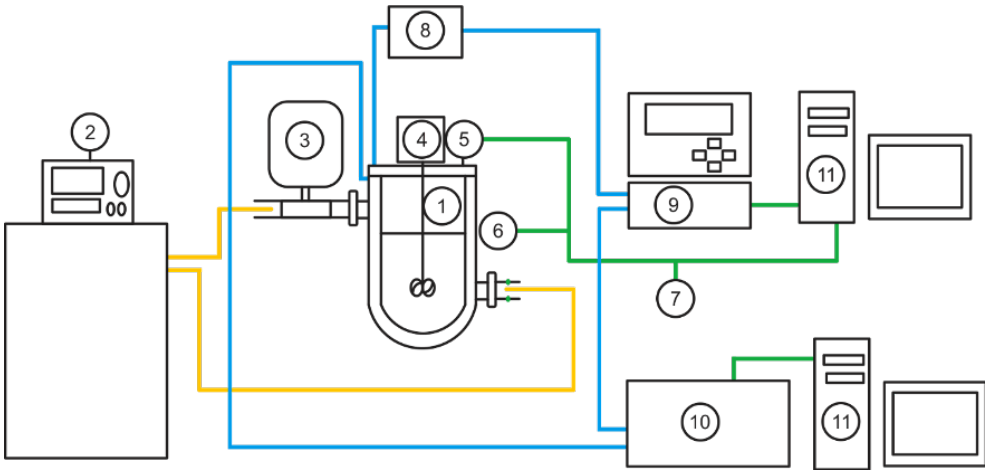

Fig. 1. Schematic diagram of experimental equipment: 1) crystallizer, 2) thermal bath, 3) refrigerant flowrate valve, 4) agitator, 5, 6 and 7) thermocouples, 8) peristaltic pump, 9) densitometer, 10) Mastersizer and 11) computer equipment.

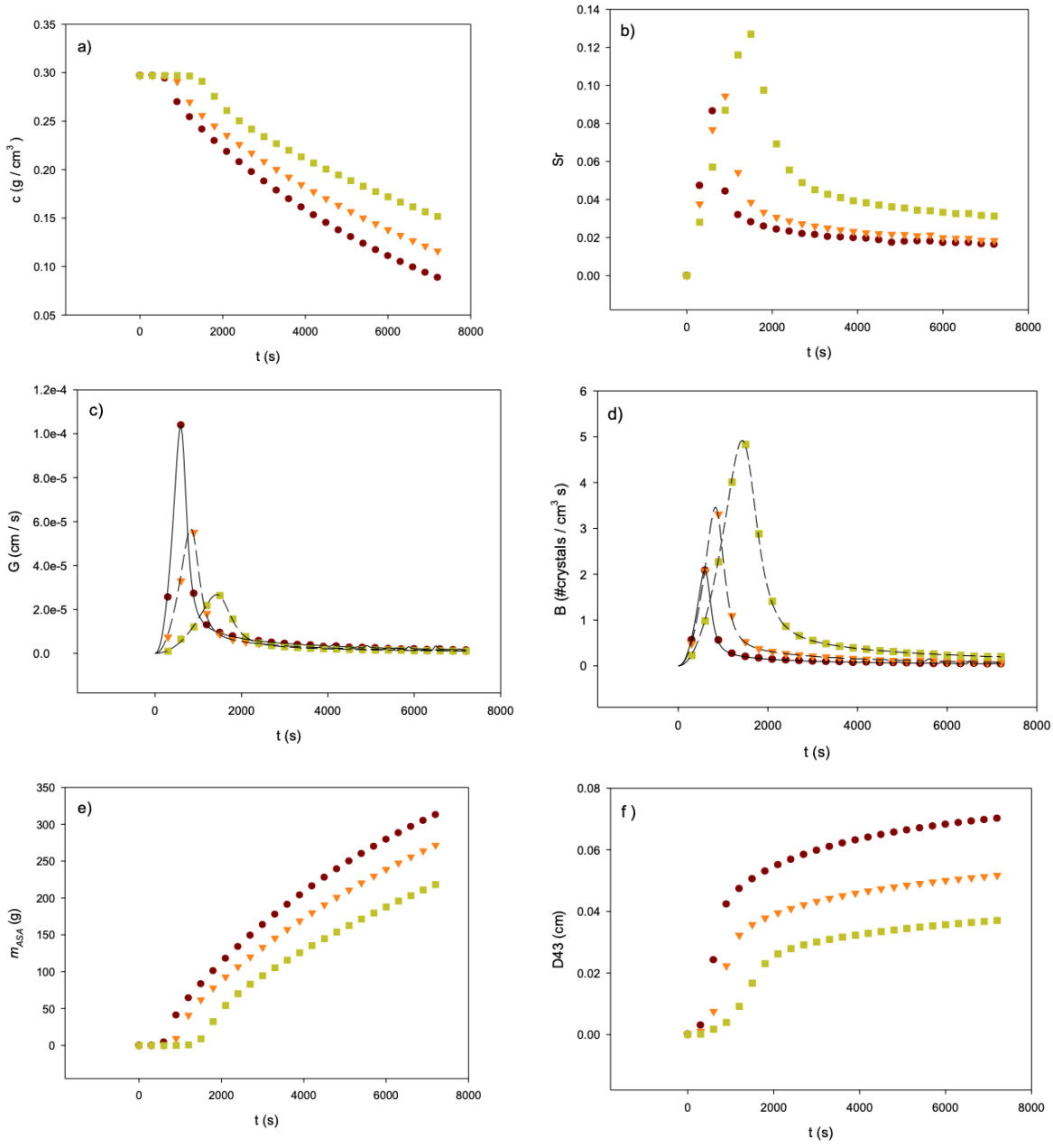

Fig. 2. Experimental profiles of a) concentration, b) relative supersaturation, c) growth rate, d) nucleation rate, e) mass of ASA and f) crystal size $D_{4,3}$ for a saturated solution prepared at 0.2970 g/cm^3 and cooling rates of: ● 15 K/h, ▼ 12 K/h, and ■ 9 K/h. Calculated profiles, for G and B, at cooling rates of − 15 K/h, − − 12 K/h, and - - 9 K/h.

The maximum growth rates achieved at each cooling rate go from 2.65×10^{-5} to 1.03×10^{-4} (cm/s) and the maximum nucleation rates achieved at each cooling rate go from 2 to 5 (#crystals/cm^3 s). These results show that an increment in cooling rate favors growth but inhibits nucleation; therefore, the overall result is a batch with greater mass, transferred from the liquid phase to the solid phase (Fig. 2e), and crystals of larger size (Fig. 2f). Table 2 shows the experimental values (reported every 600 seconds) for the average runs with saturated solution at 0.2970 g/cm^3 and cooling rate of 9 K/h.

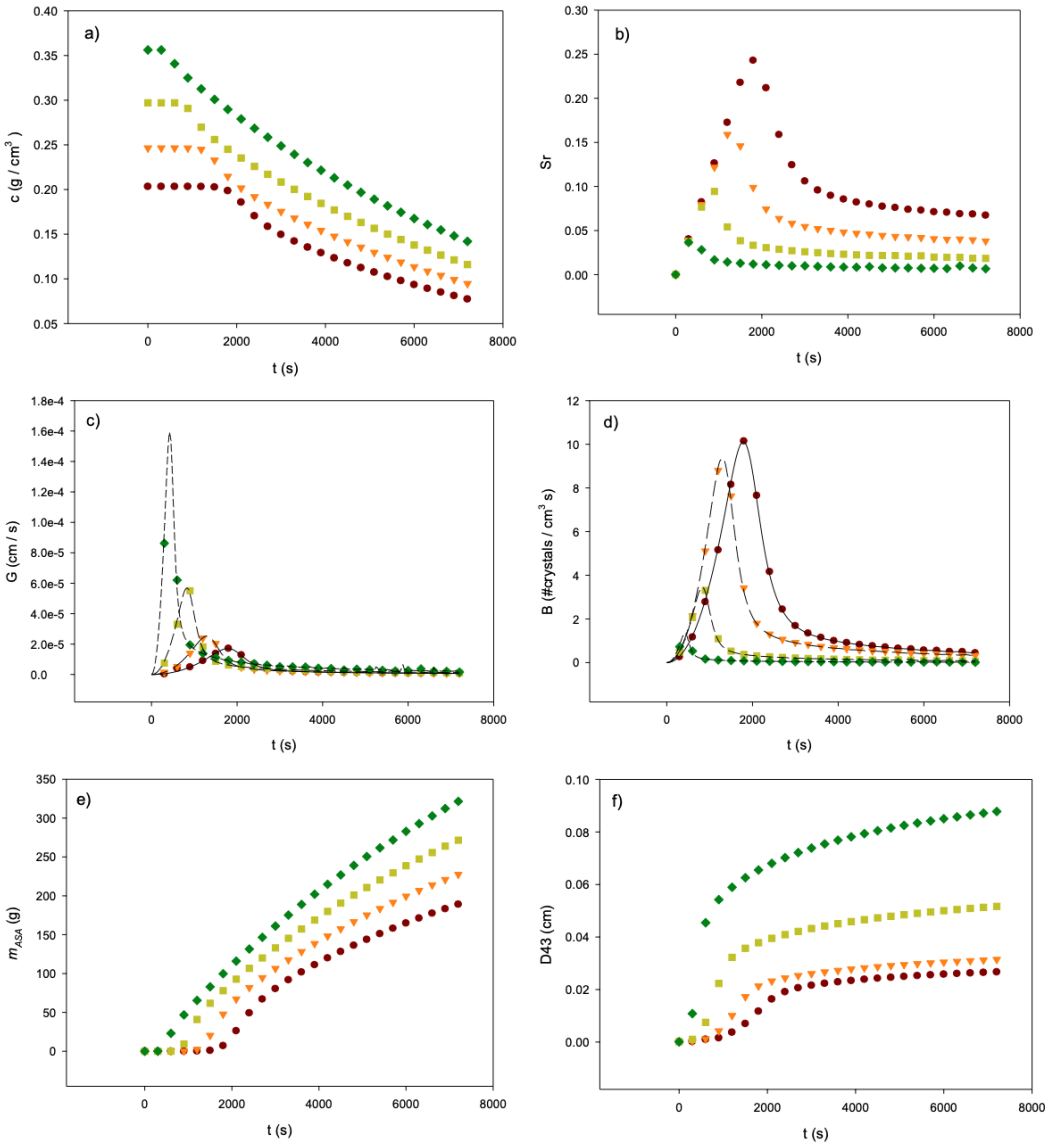

Fig. 3. Experimental profiles of a) concentration, b) relative supersaturation, c) growth rate, d) nucleation rate, e) mass of ASA and f) crystal size D43 with a constant cooling rate of 12 K/h, and saturations concentrations of: ● 0.2031 g/cm^3, ▼ 0.2464 g/cm^3, ■ 0.2970 g/cm^3 and ◆ 0.3562 g/cm^3. Calculated profiles, for G and B, at saturation concentrations of – 0.2031 g/cm^3, – – 0.2464 g/cm^3, - - 0.2970 g/cm^3 and ⋯ 0.3562 g/cm^3.

Fig. 3a shows the concentration profiles of four experiments initially saturated at different values and cooled at constant rate of 12 K/h. Experiments with low saturation concentration present a larger lag before nucleation appear. Again, this lag generates an increment in the relative saturation. At a low relative saturation, growth is improved, as shown in Fig. 3c. The maximum growth rates go from 2.0×10^{-5} to 1.6×10^{-4} (cm/s). The maximum nucleation values are reached when the relative saturation reaches the maximum value too. Fig. 3d shows that the maximum nucleation rates achieved go from 1.8 to 10.5 (#crystals/cm^3 s). Solutions with initial greater saturation concentration produce batches with greater mass and larger crystal size as shown in Figures 3e and 3f. It is clear in this set of experiments, that the two hours operation time was not enough to allow the complete mass transfer from the liquid phase to the solid phase.

Table 2. Experimental results for a run with initial saturation concentration of 0.2970 g/cm^3 and cooling rate of 9 K/h.

Time s	Temperature K	Concentration g/cm^3	Nucleation #crystals/cm^{3}s	Growth cm/s
0	308.15	0.2970	0.0008	4.6001E-09
600	306.65	0.2970	1.0853	5.8073E-06
1200	305.15	0.2965	4.1817	2.2696E-05
1800	303.65	0.2756	2.6702	1.4520E-05
2400	302.15	0.2503	0.8320	4.5205E-06
3000	300.65	0.2340	0.5443	2.9368E-06
3600	299.15	0.2199	0.4253	2.2888E-06
4200	297.65	0.2068	0.3620	1.9431E-06
4800	296.15	0.1945	0.3118	1.6684E-06
5400	294.65	0.1828	0.2672	1.4248E-06
6000	293.15	0.1719	0.2313	1.2303E-06
6600	291.65	0.1615	0.2155	1.1427E-06
7200	290.15	0.1516	0.1985	1.0497E-06
7800	288.65	0.1423	0.1689	8.9055E-07
8400	287.15	0.1336	0.1518	7.9897E-07
9000	285.65	0.1251	0.1763	9.2368E-07
9600	284.15	0.1173	0.1422	7.4262E-07
10200	282.65	0.1096	0.1265	6.5879E-07

4.2 Kinetic parameters evaluation

The estimation of the six kinetic parameters, k_{b0}, b, E_b, k_{g0}, g, E_g can be an uncertain process, since the equations have a high degree of non-linearity, thus originating several roots for the best values of the parameters (local optimum). To reduce the search intervals, it was taken into account that according to the BCF model (Burton-Cabrera-Frank), the values of g can take values between one and two (one at high supersaturations and two at low supersaturations). Furthermore, this interval for g is similar to the one reported by Mohan and Myerson (2002) and Quintana-Hernández, *et al*. (2008) for other systems. In order to facilitate the convergence of the proposed solution algorithm, in this work the search interval of the growth exponent was expanded from 0.5 to 3.

Regarding the search interval for the nucleation exponent, Garside and Shah (1980) reported a kinetic crystallization index defined by the ratio of the nucleation and growth exponents, $i = b/g$. They found that for different crystallization systems the index interval took values between 1 and 2. Using this interval and the proposed limits for g, the interval for parameter b was set from 0.5 to 6.

Table 3 shows the results obtained for the optimization of the kinetic parameters obtained for different cooling rate with a constant initial saturation concentration of 0.2970 g/cm^3. The activation energy parameters for both nucleation and growth decrease when the cooling rate increases. On the other hand, the frequency factor of growth increases and the frequency factor of nucleation decreases when the cooling rate increases. The combined effect of activation energy and frequency factor generate higher growing rates and lower nucleation rates when cooling rate increases. In addition, the exponents of nucleation and growth slightly increase when cooling rate increases. The average value of g, including all cases shown on Tables 3, was close to two, which could be an indication of predominant mechanism of surface diffusion during the growing period (Zhang et. al. 2017).

Regarding to the exponent of the nucleation rate, the average value of b was two, which according to Garside and Daver (1980) would suggest the presence of primary nucleation. Larger values for b have been reported in the literature. Those larger values have been associated with other process variables or transport mechanisms. Zauner and Jones (2000) found values between 3.9 and 7.0 for the crystallization of calcium oxalate with a great dependence of the stirring speed. Garcide and Davey (1980) reported that the solution density also had an influence on the nucleation rate. They reported values greater that four when secondary nucleation was dominant.

Table 3. Correlated nucleation and growth kinetics for solutions at different cooling rate and constant saturation concentration (0.2970 g/cm^3).

R_c	k_{b0} x10^{-4}	b	E_b	k_{g0}	g	E_g
K/h	# crystals/cm^3 s		J/mol	cm/s		J/mol
9	77.5540	2.0132	19833	3.7161	2.0141	19509
12	6.0157	2.0347	12787	5.4372	2.0350	17269
15	2.2022	2.0516	10782	10.7030	2.0782	16416

Table 4. Correlated nucleation and growth kinetics for solutions at different saturation concentration and cooled at constant rate of 12 K/h.

c	k_b x10^{-4}	b	E_b	k_g	g	E_g
g/cm^3	# crystals/cm^3 s		J/mol	cm/ s		J/mol
0.2031	30.0210	2.0401	18025	1.9467	2.0517	21231
0.2464	12.0800	2.0374	14335	2.4027	2.0386	19290
0.2970	6.0157	2.0347	12787	5.4372	2.0350	17269
0.3562	5.7101	2.0395	11464	9.1385	2.0248	12389

Table 4 shows the results obtained for the optimization of the kinetic parameters obtained for different saturation concentration cooled at constant rate of 12 K/h. The activation energy parameters for both nucleation and growth decrease when the solution concentration increases. This means that nucleation and growth are favored when more molecules are available in the solution. On the other hand, the frequency factor of growth increases and the frequency factor of nucleation decreases when saturation concentration increases. The combined effect of activation energy and frequency factor generate higher growing rates and lower nucleation rates when saturation concentration increases. In addition, the exponents of nucleation and growth slightly decrease when saturation concentration increases. The average values of b and g, including all cases shown on Tables 4, were close to two, which could be an indication of predominant mechanism of primary nucleation and surface diffusion during the growing period, as described before.

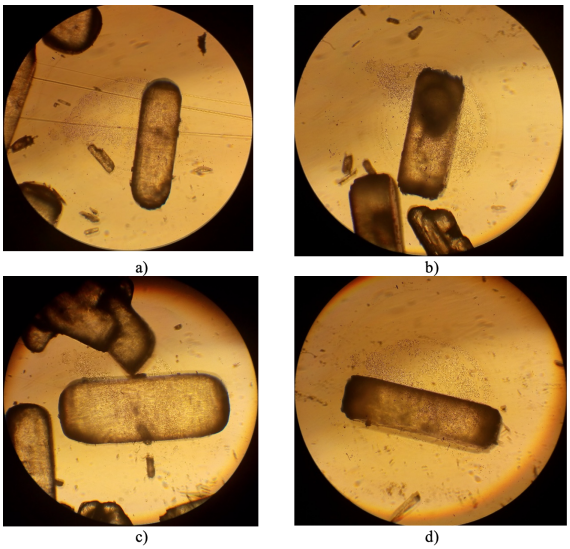

Fig. 4. Microscopic images of ASA crystals obtained at a cooling rate of 12 K/h and different initial saturation concentration: a) 0.2031 g/cm^3, b) 0.2463 g/cm^3, c) 0.2970 and d) 0.3562 g/cm^3 (visual field diameter 500 μm).

4.3 Morphological analysis

ASA crystals have a tetragonal (prism-shape) habit with dimensions a, b and c ($a > b$ and $c = b$). Fig. 4 shows microscopic images of ASA crystals obtained at different experimental conditions and Table 5 shows the dimensions of the biggest crystal shown at each image. These images show no qualitative difference in crystal habit (all crystals present similar habit: prism-shape). Fig. 4c shows the image of an ASA crystal with dimensions $a = 300\mu m$, and $b = 123\mu$m.

The experimental specific shape factors can be calculated with eqs. (12)-(14) using the second largest dimension, b, as the characteristic dimension, L (Jones, 2002; Mulling, 2001). The surface shape factor, k_s is equal to $2 + 4a/b = 11.75$; and the volume shape factor, k_v is equal to $a/b = 2.44$. Therefore, the specific shape factor, F is equal to $4 + 2b/a = 4.82$. Table 5 presents the specific shape factors for the crystals obtained at other conditions.

Table 5. Crystal dimensions and specific factors for different experimental conditions, corresponding to images on Figure 4.

Fig	b μm	a μm	k_s	k_v	F_{exp}	F_c	*Error* %
a)	84.61	207.69	11.82	2.45	4.81	4.83	0.42
b)	87.50	213.23	12.09	2.52	4.82	4.82	0
c)	123.07	300.00	11.75	2.44	4.82	4.82	0
d)	85.71	210.71	11.83	2.46	4.81	4.83	0.42

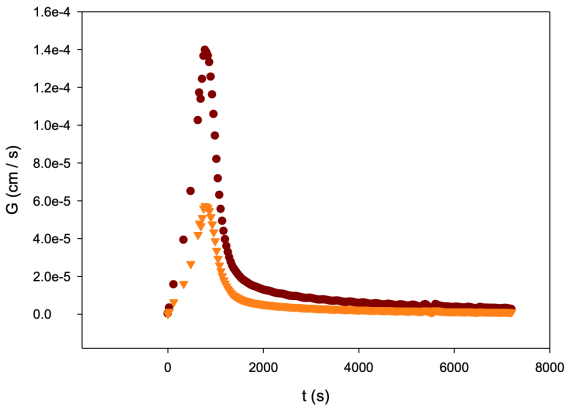

Fig. 5. ASA crystal facet growth rates for an experiment with initial saturation condition of 0.2970 g/cm^3 and cooling rate of 12 K/h, ● (010) and ▼ (100).

Another approach to evaluate the specific shape factor is minimizing the difference between the growth rate profiles evaluated with the measurements given by the Master Sizer (Eq. 26) and the growth rate calculated based on mass flux transferred, Eq. (27).

$$G = \frac{\left(\frac{\Delta m_{ASA}}{\Delta t}\right) F}{3\rho_{ASA} M_2 V_s} \tag{27}$$

Table 5 shows the specific shape factors evaluated minimizing the differences between Eq. 26 and Eq. 27. These calculated values were very close to those experimentally calculated. The overall difference was less than 0.5%. On the other hand, the results showed that the specific shape factors were similar in all experiments regardless of the operation conditions. Therefore, large morphological differences between crystals obtained at the conditions analyzed in this study were not expected.

Finally, Fig. 5 shows the growth rate of the crystal facets (100), (010) and (001) as function of time for an experiment with initial saturation condition of 0.2970 g/cm^3 and cooling rate of 12 K/h. Facet (100) has dimensions bxb; facets (010) and (001) have dimensions axb. For calculating facet growth rates, prism-shape crystal dimensions were taken as $b = D_{43}$ and $a = 2b/(F-4)$. Facets (010) and (001) are similar; therefore, they have equal growth rate. The results show that facet (010) grows up to 2.43 times faster than facet (100). This growing ratio preserves the prism-shape habit in all crystals.

Conclusions

Nucleation and growth rates for the system acetylsalicylic acid-ethanol were successfully evaluated from experimental data at different operation conditions. Kinetic parameters were estimated with a nonlinear optimization algorithm and experimental results of solution concentration profiles. The results of the mathematical model were compared against the experimental information finding good agreement. In addition, it was found that an increment in cooling rate enhanced growth but inhibited nucleation. Similar results were obtained for an increment in solution initial saturation concentration. The analysis of the kinetic exponents suggested crystal growth was dominated by surface diffusional effects and formation of new nuclei was dominated by primary nucleation. The crystal images showed no morphological differences between crystals due to different operation conditions. Specific shape factor evaluation confirmed the absence of morphological changes in the ASA crystals.

References

Bolaños-Reynoso, E., Sánchez-Sánchez, K. B, López-Zamora, L. and Ricárdez-Sandoval, L. (2018). A study on empirical and mechanistic approaches for modelling cane sugar crystallization. *Revista Mexicana de Ingeniería Química 17*, 289-406. https://doi.org/10.24275/10.24275/uam/izt/dcbi/revmexingquim/2018v17n2/Bolanos

Eder, R. J. P., Schrank, S., Besenhard, M. O., Roblegg, E., Woelfler, G. H. and Khinast, J. G. (2012). Continous sonocrystallization of acetylsalicylic acid (asa): control of crystal size. *Crystal Growth and Desing 12*, 4733-4738. https://doi.org/10.1021/cg201567y

Frawley, P. J., Mitchell, N. A., Ó'Ciardhá, C. T., Hutton, K.W. (2012). The effects of supersaturation, temperature, agitation and seed surface area on the secondary nucleation of paracetamol in ethanol solutions. *Chemical Engineering Science 75*, 183-197. http://dx.doi.org/10.1016/j.ces.2012.03.041

Garcide, J. and Davey, R. J. (1980). Secondary contact nucleation: Kinetics, growth and scale-up. *Chemical Engineering Communications 4*, 393-399. https://doi.org/10.1080/00986448008935918

Garcide, J. and Shah, M. N. (1980). Crystallization kinetics from MSMPR crystallizers. *Industrial and Engineering Chemistry Process Design and Development 19*, 509-514. http://doi.org/10.1021/i260076a001

Halburt, H. and Katz, S. (1964). Some problems in particle technology. *Chemical Engineering Science 19*, 555-574.

Jerauld, G. R., Vasatis, Y. and Doherty, M. F. (1983). Simple conditions for the appearance of sustained oscillations in continuous crystallizers. *Chemical Engineering Science 38*, 1675-1681. https://doi.org/10.1016/0009-2509(83)85024-6

Jin, X., Chenglin, L., Mengjie, L., Mengxing, L., Youfa, J., Ping, L., Jianguo, Y. and Sohrab, R. (2019). Secondary nucleation and growth kinetics of aluminum hydroxide crystallization from potassium aluminate solution. *Journal of Crystal Growth 507*, 232-240. https://doi.org/10.1016/j.jerysgro.2018.11.027

Jones, A. G. (2002). *Crystallization Process Systems*. First ed. Oxford: Butterworth-Heinemann, United Kingdom.

Kashchiev, D., Borissova, A., Hammond, R.B. and Roberts, K. (2010). Dependence of the critical undercooling for crystallization on the cooling rate. *J. Phys. Chem. B. 114*, 5441-5446. https://doi.org/10.1021/jp100202m

Liang, B. and Hartel, R.W. (1991). Techniques for developing nucleation and growth kinetics from MSMPR data for sucrose crystallization in the presence of growth rate dispersion. *Journal of Crystal Growth 108*, 129-142. https://doi.org/10.1016/0022-0248(91)90361-8

Maia, G.D. and Giulietti, M. (2008). Solubility of acetylsalicylic acid in etanol, acetone, propylene glycol, and 2-propanol. *J. Chem. Eng. Data 53*, 256 - 258. https://doi.org/10.1021/je7005693

Medina-Galván, X. M. (2018). *Medición del ancho de la zona metaestable de soluciones de ácido acetilsalicílico-etanol*. Tesis de Maestría en Ciencias en Ingeniería Química, Instituto Tecnológico Nacional de México en Celaya, México.

Mulling, J.W. (2001). *Crystallization*. 4th. Edition. Oxford: Butterworth-Heinemann, United Kingdom.

Mohan, R. and Myerson, A.S. (2002). Growth kinetics: a thermodynamic approach. *Chemical Engineering Science 57*, 4277 - 4285. https://doi.org/10.1016/s0009-2509(02)00344-5

Monaco, L. A. and Rosenberger, F. (1993). Growth an etching kinetics of tetragonal lysozyme. *Journal of Crystal Growth 129*, 465-484. https://doi.org/10.1016/0022-0248(93)90481-B

O'Hara, M. and Reid, R. C. (1973). *Modelling Crystal Growth Rates from Solution*. Englewood Cliffs¸Prentice-Hall, United States.

Polat, S., and Sayan, P. (2017). Characterization and kinetics of calcium sulfate dihydrate crystallization in the presence of trimesic acid. *Asia-Pacific Journal of Chemical Engineering 12*, 391-399. https://doi.org/10.1002/apj.2081

Qiu, Y. and Rasmuson, A. C. (1994). Estimation of crystallization kinetics from bath cooling experiments. *AIChE Journal 40*, 799-812. https://doi.org/10.1002/aic.690400507

Quintana-Hernández, P. A., Bolaños, E., Saucedo, L. and Miranda, C. B. (2004). Mathematical modeling and kinetic parameter estimation in batch crystallization. *AIChE Journal 50*, 1407-1417. https://doi.org/10.1002/aic.10133

Quintana-Hernández, P. A., Uribe-Martínez, B., Rico-Ramírez, V., and Bolaños-Reynoso, E. (2008). Análisis comparativo de ecuaciones cinéticas tipo ley de potencia y difusión-integración en la cristalización por enfriamiento de azúcar de caña. *Revista Mexicana de Ingeniería Química 7*, 171-182.

Quintana-Hernández, P. A., Díaz-Pérez, G.., Rico-Ramírez, V., and Salcedo-Estrada, L. I. (2016). Metastable zone width measurements of adipic acid-water solutions. *Revista Mexicana de Ingeniería Química 15*, 1008-1018. https://rmiq.org/ojs311/index.php/rmiq/article/view/1153

Randolph, A. D. and Larson, M. A. (1988). *Theory of Particulate Processes*. Second edition. San Diego: Academic Press INC., USA.

Rawlings, J. B., Sink, C.W. and Miller, S. M. (2002). *Control of Crystallization Processes, Handbook of Industrial Crystallization* (Second Edition). Pp. 201-230. Buttemworth Heinemann, Elsevier, United Kingdom. https://doi.org/10.1016/B978-075067012-8/50011-2

Sanchez-Sanchez, K. B., Bolaños-Reynoso, E. and Urrea-Garcia, G. R. (2017). Analysis of operation conditions for sugar cane batch crystallization based on MSZW mechanistic kinetic models. *Revista Mexicana de Ingeniería Química 16*, 1029-1052. https://rmiq.org/ojs311/index.php/rmiq/article/view/1099

Sanchez-Sanchez, K. B., Bolaños-Reynoso, E., Mendez-Contreras, J. M. and Cerecero-Enriquez, R. (2020). Effects of agitation rates over metastable zone width (MSZW) of concentration for cane sugar crystallization. *Revista Mexicana de Ingeniería Química 19*, 507-520. www.rmiq.org/ojs311/index.php/rmiq/article/view/809

Singh, M. R., and Ramkrishna, D. (2013). A comprehensive approach to predicting crystal morphology distributions with population balances. *Crystal Growth and Design 13*, 1397-1411. https://doi.org/10.1021/cg301851g

Söhnel, O. and Garside, J. (1991). *Precipitation*. Oxford: Butterworth-Heinemann, United Kingdom.

Wey, J. S. (1985). Analysis of bath crystallization processes. *Chemical Engineering Communications 35*, 231 - 252. https://doi.org/10.1080/00986448508911230

Xiong, L., Zhou, L., Zhang, X., Zhang, M., Hou, B., Bao, Y., Du, W., Zhang, S. and Yim, Q. (2018). Determination of metastable zone width and nucleation behavior of aspirin in acetic acid and acetic anhydride binary solvent mixture. *Journal of Molecular Liquids 269*, 805-815. https://doi.org/10.1016/j.molliq.2018.08.055

Zauner, R. and Jones, A. G. (2000). Determination of nucleation, growth agglomeration and disruption kinetics from experimental precipitation data: The calcium oxalate system. *Chemical Engineering Science 55*, 4219-4232. https://doi.org/10.1016/S0009-2509(00)00059-2

Zhang, X. Z., Qian, G. and Zhou, X. (2017). Kinetic modeling on batch-cooling crystallization of zinc lactate: The influence of malic acid. *Journal of Crystal Growth 463*, 162-167. https://doi.org/10.1016/j.jcrysgro.2017.02.023